Mechanism and Machine Theory 184 (2023) 105286

Contents lists available at ScienceDirect

Mechanism and Machine Theory

journal homepage: www.elsevier.com/locate/mechmt

Research paper

Point to point time optimal handling of unmounted rigid objects and liquid-filled containers

Hubert Gattringer [a], Andreas Müller [a,*], Simon Weitzhofer [b], Markus Schörgenhumer [b]

[a] Johannes Kepler University Linz, Linz, Austria
[b] Linz Center of Mechatronics GmbH, Linz, Austria

ARTICLE INFO

Keywords:
Trajectory optimization
Point to point motion
Object handling
Robot dynamics
Liquid sloshing simulation

ABSTRACT

Time optimal handling of parts loosely placed at the end-effector (EE) of a robot, known as waiter motion problem, has high practical relevance, which becomes more challenging if the object is a liquid-filled container. The waiter motion problem was often restricted to a time-optimal path following problem, which limits the flexibility and task efficiency. To overcome this restriction, in this paper, the general point to point (PtP) time-optimal motion planning problem is formulated and solved with a multiple shooting method. The formulation includes all relevant dynamic effects (joint friction, contact, motor limits, etc.) assuming rigid behavior of the robot as well as of the object placed at the EE. The trajectory is C^2-continuous, avoiding bang–bang behavior of motor torques. The CasADi framework and the Ipopt solver are used for numerical computations. The reported experimental results confirm applicability of the trajectory to real robotic setup in case of rigid objects. Further, handling of containers filled with liquid is addressed. Experiments are compared with numerical results obtained with SPH particle simulation. Experiment and simulation indicate that sloshing effects must be taken into account in the control formulation.

1. Introduction

Manipulation of objects with industrial robots is a central task in factory automation, with a broad range of applications involving rigid objects, flexible bodies, or even liquid-filled containers. Ideally, the handling procedure involves the handling of rigidly grasped rigid objects. Clearly, a key element here is the stable grasp of the part to be manipulated. Recent research addressed the problem of grasping flexible objects. A problem with higher practical relevance is the handling of rigid objects that are not rigidly fixed to the robot. The parts are for instance 'affixed' to the robot by means of suction grippers or loosely placed in a container or at a hold. The hold is thus achieved via force closure. When using suction grippers, for instance, the part is pushed towards the EE by the suction force that in turn produces a tangential force due to friction, while for loosely placed parts the net normal force is only due to gravitation and EE acceleration. Fig. 1 shows a situation, where several cups are placed on an EE-fixed tray. To ensure efficiency, the handling task must be performed within the shortest time possible. In case of rigidly grasped parts, the minimum time is dictated by the robotic manipulator. However, if the objects are only attached to the robot via force closure, limits on the contact force must be taken into account for the time-optimal motion planning. This problem is known as the 'waiter motion problem' [1]. This terminology stems from the observation that manipulating unmounted parts resembles the task of a waiter: transporting glasses, dishes, etc. placed at a tray from the restaurant's kitchen to the customer's table as fast as possible. In a number of publications,

* Corresponding author.
E-mail addresses: hubert.gattringer@jku.at (H. Gattringer), a.mueller@jku.at (A. Müller), simon.weitzhofer@lcm.at (S. Weitzhofer), markus.schoergenhumer@lcm.at (M. Schörgenhumer).

https://doi.org/10.1016/j.mechmachtheory.2023.105286
Received 13 December 2022; Received in revised form 2 February 2023; Accepted 6 February 2023
Available online 17 February 2023

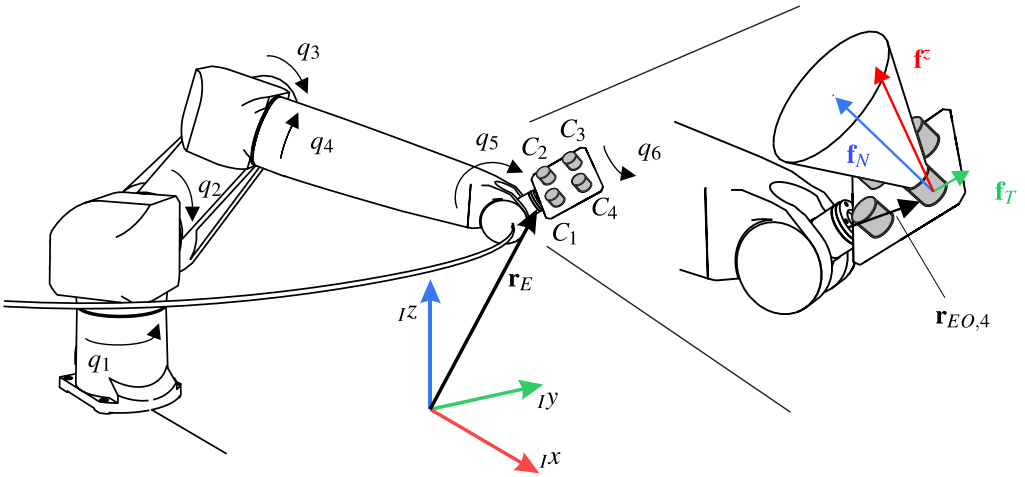

Fig. 1. Waiter motion; industrial robot and 4 cups; friction cone in detail.

the waiter motion problem has been formulated as a path-following problem, i.e. the geometric path of the Cartesian position of object or EE is prescribed, and the task is to follow this path in minimum time while optimally aligning the EE. In [2], the numerical integration method was used, where the optimal switching points are determined to switch from maximal acceleration to deceleration. The path following problem was solved in [3] with a dynamic programming method. In this publication experimental results of a real system operating at the physical limits were reported. A critical aspect of these methods is that it leads to a bang–bang control, i.e. the drive torques alternate between their maximal and minimal values. A convex formulation of the problem was used in [4] where the position and the orientation of the object/EE are prescribed, and constraints for avoiding tip-over are included. A formulation as convex second-order cone program was introduced in [5] to solve the waiter motion problem using the direct transcription method. These methods rely on a convex formulation obtained by omitting joint friction. Nagy et al. [6] extended the problem formulation with a non-convex jerk constraints to avoid unwanted oscillations during the motion. A direct multiple shooting method was applied to the problem including joint friction, and experimental results were reported in [7,8]. Including joint friction is decisive in order to obtain realistic trajectories which can actually be executed on the real robot.

In most applications, the path is not prescribed by the handling task, rather the start and terminal poses are defined. Therefore, and to fully exploit the capability and to ensure flexibility of the robot, the realistic waiter motion problem is described as a point-to-point (PtP) optimal control problem. This PtP problem was addressed in a few publications. In [9], a two step optimization procedure was proposed where intermediate points were introduced between which the optimal path following problem is solved. Time-optimal transportation of goods using suction cups is addressed in [10], which is a continuation of [11] where the tasks of manipulating loosely placed objects on a tray underneath an obstacle was discussed. The unilateral contact and the friction cone condition are the peculiarities of the waiter motion problem. In context of general trajectory optimization, they have been included in [12,13]. In [13], the non-sliding constraints are incorporated into a second order cone problem which is solved using a sequential solution algorithm. To simplify the non-linear time-optimal path following problem, the friction cone constraints were linearized in [2]. A different approach for sloshing-free liquid transportation on a conveyor belt is presented in [14]. There, speed dependent motion profiles are optimized that minimize residual vibrations. A sloshing-free solution for manipulation liquids with robots is part of [15]. Exponential filters for desired trajectories are used to counteract the sloshing motion. Additionally, an orientation compensation mechanism is explained to align the modeled pendulums with the vessel. However, no time optimization for the motion is presented. A different approach for sloshing-free robot trajectory generation can be found in [16]. The authors model the liquid filled vessel as a spherical pendulum and study the requirements for sloshing free motion of a point mass model. Again, no time optimization is done.

In this paper, a numerical approach for the solution of the time-optimal PtP waiter motion problem and experimental results are presented, with the primary focus on rigid objects placed at the EE. In the authors previous publications, e.g. [8], only the path following waiter motion problem is solved, where the geometric path is predefined (so that the motion is described by a path parameter), and the optimal trajectory along this path is computed. The robot itself is assumed to be rigid, i.e., the finite stiffness of the arms and EE, as well as the compliance of joints and drives are neglected. Therefore, elastic effects and vibration dynamics are not included in the optimization. Under these assumptions, the optimal control problem includes all task constraints (normal and friction forces of objects), in order to prevent twist and tip over of the objects, and all limitations of the robot (max. speed, acceleration, jerk, and drive torque). The jerk of the joint coordinates is used as the control input to the optimization problem. The time-optimal trajectory is thus C^2 continuous (continuous acceleration), and does not cause jumps of the drive torques. The problem formulation includes viscous friction, and thus yields a non-convex optimization problem. The latter is solved numerically with a direct multiple shooting method that is implemented in the CasADi framework [17], and the optimization problem is solved with

Ipopt [18]. Feasibility of the time-optimal PtP motion is verified experimentally, which confirms that the robot can in fact operate almost at the physical limits.

In various industrial applications the manipulated object loosely placed at the EE is not a rigid body, but rather a possibly open, liquid-filled container. Then the complex sloshing dynamics plays a crucial role, and must be appropriately accounted for. Capturing the sloshing dynamics is vital in many industrial applications [19], including vibration dampers based on liquid masses [20], sloshing of fuel in vehicle tanks [21], automated handling of liquid-filled containers [22], and robotic automation [23–27]. Analytic and empirical models were derived to this end [28], which have limited generalizability, however, particularly with respect to the container geometry and the excitation (motion) for general 3D scenarios. Numerical methods from computational fluid dynamics (CFD) provide a generally applicable but computationally expensive alternative, including mesh-based techniques, e.g. finite element or finite volume methods [29–31], and meshless methods, e.g. particle-based methods [32–34], which allow for analyzing sloshing dynamics [35]. A main challenge is to appropriately account for the free fluid surface including sloshing and possibly splashing effects. The latter can be handled by Lagrangian, particle-based methods more naturally. A problematic aspect is the consistent treatment of (wall) boundary conditions, however. The crucial point of all mentioned computational approaches is that they cannot be included in the computational schemes for solving the optimal control problem due to their computational complexity. Unfortunately, simple pendulum and mass–spring–damper models [26,27,36] do not allow for accurate modeling of sloshing as they are valid for planar motions only. Nevertheless, even if the sloshing dynamics cannot be included directly in the numerical trajectory optimization scheme, CFD simulation methods can be used to check and verify applicability of the obtained trajectories a posteriori. This is done in the present paper. To this end, numerical 3D free-surface flow simulations are performed using the particle-based Smoothed Particle Hydrodynamics (SPH) method that was originally introduced in [37] and applied to free surface flows in [38], which is applicable to solid and fluid mechanics [39,40]. A co-simulation setup of the multibody simulation tool HOTINT [41] and the particle simulator LIGGGHTS [42], originally developed for the analysis of fluid–structure interaction problems [43,44], is used. This is a further contribution of this paper. To the best of the authors knowledge, there are no publications that address the time-optimal waiter motion problem for PtP trajectories in combination with a validation by CFD simulations.

The paper is organized as follows. Section 2 presents the dynamic model of the robot and the objects, as well as the calculation of contact forces. The task constraints for moving loosely placed objects on a tray are combined in Section 3. The time optimal point to point motion planning is the focus of Section 4, and the corresponding experimental results are presented in Section 5. The extension to the handling of liquid filled containers concludes the paper in Section 6.

2. Inverse dynamics model

Basis for the optimal control problem is the inverse dynamics model of the controlled robot, which serves to deliver the vector of motor torques, denoted with $\mathbf{Q}_{\mathrm{M}}(t)$ for a given motion of the robot, represented by the vector of joint variables $\mathbf{q}(t)$. Moreover, since this inverse dynamics model is used to evaluate the constraints on the motor torques, the identification of the corresponding parameters is crucial. Not all dynamic parameters are independently identifiable, only a set of so-called base parameters can be identified [8,45,46]. This is sufficient to obtain a validated inverse dynamics model. The latter can be written in the form

$$\mathbf{Q}_{\mathrm{M}} = \boldsymbol{\Theta}(\mathbf{q}, \dot{\mathbf{q}}, \ddot{\mathbf{q}})\mathbf{p} \tag{1}$$

where $\boldsymbol{\Theta}$ is the regressor matrix as function of state $\mathbf{q}, \dot{\mathbf{q}}$ and its derivatives, and the vector $\mathbf{p}$ comprises the identifiable base parameters. Since (1) is linear in the base parameters $\mathbf{p}$, it provides the basis for identification. To this end, $\boldsymbol{\Theta}(\mathbf{q}, \dot{\mathbf{q}}, \ddot{\mathbf{q}})$ and $\mathbf{Q}_{\mathrm{M}}$ are measured along optimized identification trajectories $\mathbf{q}(t)$, and the corresponding regression problem is solved.

An important aspect for the efficient generation of EOM and the corresponding inverse dynamics model is to follow a modular modeling approach. This is particularly relevant in order to admit easy substitution of the equations accounting for the dynamics of the parts to be handled. The latter admits representing complicated contact geometries but also internal dynamics as in case of containers filled with liquid [26,27,36]. Depending on the environmental conditions, the subsystem representing the object to be handled could also take into account aerodynamic forces. Denote with N_{Obj} the number of objects to be handled. The dynamics model of the ith manipulated object, which is loosely placed at the EE, has the general form

$$\mathbf{Q}_i^z = \mathbf{M}_i\dot{\mathbf{y}}_i + \mathbf{G}_i\dot{\mathbf{y}}_i - \mathbf{Q}_i, \;\; i = 1, \ldots, N_{\mathrm{Obj}} \tag{2}$$

where $\mathbf{M}_i$ is the generalized mass matrix, $\mathbf{G}_i\dot{\mathbf{y}}_i$ is the vector of generalized Coriolis and centrifugal forces, and $\mathbf{Q}_i$ represents generalized forces due to gravity and further external loads. Further, $\dot{\mathbf{y}}_i$ is the vector of generalized velocities of the object, and $\mathbf{Q}_i^z$ is the vector of generalized constraint forces. The generalized velocities $\dot{\mathbf{y}}_i$ are independent, and the system (2) serves as EOM of the separated object. In general, the DOF of this subsystem depends on the object and the dynamic effects represented [8]. In the following the ith handled object is a single rigid body. Then $\dot{\mathbf{y}}_i = (\mathbf{v}_i^T \;\; \boldsymbol{\omega}_i^T)^T$ is the rigid body twist, and $\mathbf{Q}_i^z = \left(\mathbf{f}_i^{zT} \;\; \mathbf{M}_i^{zT}\right)^T$ is the contact wrench, with constraint force $\mathbf{f}_i^z$ and torque $\mathbf{M}_i^z$, respectively. More precisely, $\mathbf{v}_i$ is the velocity of the contact point of object i. If (1) represents the robot dynamics, then the overall motor torques necessary for executing a task with trajectory $\mathbf{q}_{\mathrm{d}}(t)$ are determined by the inverse dynamics model

$$\mathbf{Q}_{\mathrm{M,ff}}(\mathbf{q}_{\mathrm{d}}, \dot{\mathbf{q}}_{\mathrm{d}}, \ddot{\mathbf{q}}_{\mathrm{d}}) = \boldsymbol{\Theta}(\mathbf{q}_{\mathrm{d}}, \dot{\mathbf{q}}_{\mathrm{d}}, \ddot{\mathbf{q}}_{\mathrm{d}})\mathbf{p} + \sum_{i=1}^{N_{\mathrm{Obj}}} \left(\frac{\partial \dot{\mathbf{y}}_i}{\partial \dot{\mathbf{q}}}\right)^T \left(\mathbf{M}_i\ddot{\mathbf{y}}_i + \mathbf{G}\dot{\mathbf{y}}_i - \mathbf{Q}_i\right) \tag{3}$$

which is obtained assuming perfect contact (no slipping) of the object and EE, so that the object velocities are determined by $\dot{\mathbf{y}}_i = \frac{\partial \dot{\mathbf{y}}_i}{\partial \dot{\mathbf{q}}}\dot{\mathbf{q}}$ (see Section 3). The motor torques $\mathbf{Q}_{\mathrm{M,ff}}$ are used as feed-forward command in the model-based controller.

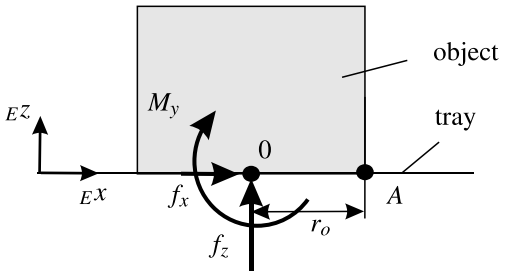

Fig. 2. Contact forces and torques between object and tray ($_E x - _E z$ view).

3. Task constraints

The overall motion must respect several constraints so to maintain contact via force closure. These are briefly summarized here, their derivations can be found in [8]. The object and the surface it is placed at are assumed to be flat. The EE-frame is introduced so that its z-axis is normal to the surface and pointing away from the surface (see Fig. 2). Denote with $\mathbf{f}_T = (f_x, f_y, 0)^T$ and $\mathbf{f}_N = (0, 0, f_z)^T$ the contact force tangential and normal to the contact plane (omitting index i), i.e. the relevant components of $\mathbf{f}_i^z$ in $\mathbf{Q}_i^z$.

Non-lifting condition: Denote with f_z the normal component of the contact force. The condition for preventing that the object lifts off the surface is $f_z \leq 0$.

Non-slipping condition: Denote with μ_0 the static friction coefficient of the object-surface contact. This must be determined experimentally, and is possibly different for the different objects. It can be identified via $\tan\rho = \mu_0$, where ρ is the angle where sliding starts. The condition for non-slipping is $\|\mathbf{f}_\mathrm{T}\| \leq -\mu_0 f_z$.

Non-tip-over condition: When the EE is accelerated, a torque is generated acting at the object. The torque depends on the contact geometry. The condition for that the object does not tip over is that this torque is less than the torque due to the normal force. For a circular footprint with radius r_0 (assumed to be the contact area) this condition is expressed as $\sqrt{M_y^2 + M_x^2} \leq -r_o f_z$, where M_x and M_y are components of the torque $\mathbf{M}_i^z$ as part of $\mathbf{Q}_i^z$ in (2).

Non-twisting condition: In general, also a contact torque about the surface normal is generated, which may cause the object to twist about the z-axis of the EE-frame. The condition to avoid twisting is that $|M_z| \leq M_{z,\max}$, where $M_{z,\max}$ is the maximal magnitude of the torque up to which the object sticks. M_z is again part of $\mathbf{M}_i^z$ in $\mathbf{Q}_i^z$ of (2). For a circular footprint with radius r_0, this maximal torque is $M_{z,\max} = \frac{2}{3}\mu_0 f_z r_o^3$.

4 Optimal control problem and numerical solution

A dynamic control system is formulated in terms of the state $\mathbf{x}^T = \left(\mathbf{q}^T,\ \dot{\mathbf{q}}^T,\ \ddot{\mathbf{q}}^T\right) \in \mathbb{R}^{18}$ and control input $\mathbf{u} = \dddot{\mathbf{q}} \in \mathbb{R}^6$, in the form of a simple integrator chain

$$\dot{\mathbf{x}} = \begin{bmatrix} 0 & \mathbf{I} & 0 \\ 0 & 0 & \mathbf{I} \\ 0 & 0 & 0 \end{bmatrix} \mathbf{x} + \begin{pmatrix} 0 \\ 0 \\ \mathbf{I} \end{pmatrix} \mathbf{u} =: \mathbf{f}(\mathbf{x}, \mathbf{u}). \tag{4}$$

Using the jerk as input ensures smooth torques. Let $\mathbf{q}_0$ and $\mathbf{q}_\mathrm{e}$ be the initial and terminal configuration of the robot, respectively. The optimal PtP control problem for a rest-to-rest motion is then

$$\min_{t_\mathrm{e}, \mathbf{u}} \int_0^{t_\mathrm{e}} \left(1 + k\mathbf{u}^T\mathbf{u}\right) dt \tag{5}$$

subject to

$$|\dot{\mathbf{q}}| \leq \dot{\mathbf{q}}_\mathrm{max} \tag{6}$$

$$\mathbf{u} \leq \mathbf{u}_\mathrm{max} \tag{7}$$

$$|\mathbf{Q}_\mathrm{M,ff}(\mathbf{q}, \dot{\mathbf{q}}, \ddot{\mathbf{q}})| \leq \mathbf{Q}_\mathrm{M,max} \tag{8}$$

$$\sqrt{f_{x,i}^2 + f_{y,i}^2} + \mu_0 f_{z,i} \leq 0, \quad i = 1, \ldots, N_\mathrm{Obj} \tag{9}$$

$$f_{z,i} \leq 0, \quad i = 1, \ldots, N_\mathrm{Obj} \tag{10}$$

$$\sqrt{M_{x,i}^2 + M_{y,i}^2} + r_o f_{z,i} \leq 0, \quad i = 1, \ldots, N_\mathrm{Obj} \tag{11}$$

$$|M_{z,i}| - M_{z,\max} \leq 0, \quad i = 1, \ldots, N_\mathrm{Obj} \tag{12}$$

$$\dot{\mathbf{x}} = \mathbf{f}(\mathbf{x}, \mathbf{u}) \tag{13}$$

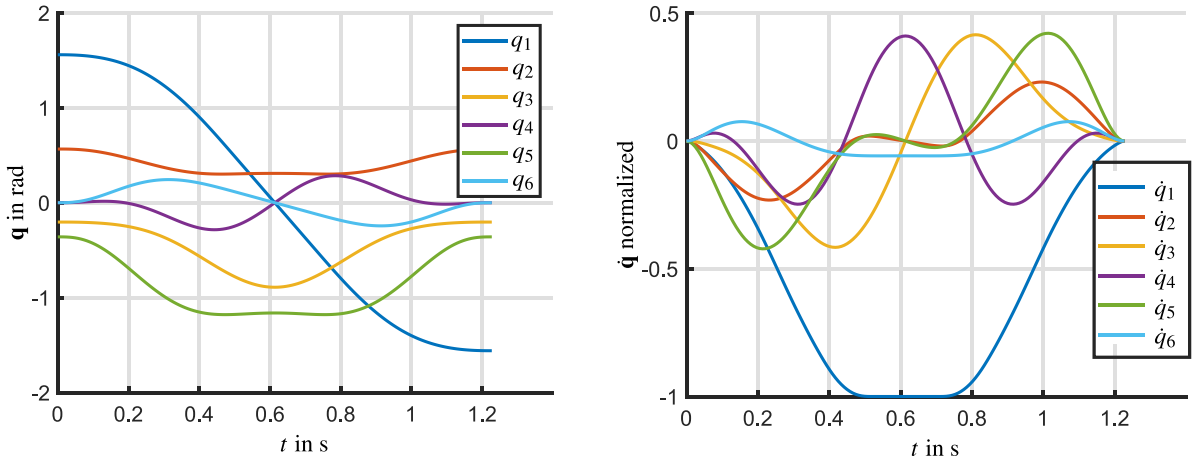

Fig. 3. Joint coordinates $\mathbf{q}$ (left) and normalized velocities $\dot{\mathbf{q}}$ (right).

$$\mathbf{q}(0) = \mathbf{q}_0, \quad \dot{\mathbf{q}}(0) = 0, \quad \ddot{\mathbf{q}}(0) = 0 \tag{14}$$

$$\mathbf{q}(t_e) = \mathbf{q}_e, \quad \dot{\mathbf{q}}(t_e) = 0, \quad \ddot{\mathbf{q}}(t_e) = 0 \tag{15}$$

where $\mathbf{Q}_{M,ff}$ is the inverse dynamics solution (3), and $\mathbf{Q}_{M,max}$ is the maximal magnitude of motor torques. Here the $\leq$ is understood componentwise. The objective function (5) accounts for execution time as well as smoothness of the trajectory. The priority of either goal is encoded in the weighting factor k ($k = 0$ implies time-optimal motion).

There are various methods for solving optimal control problems. Here it was solved with a multiple shooting method using $N = 150$ shooting intervals. The ODE (13) and the objective function (5) are integrated numerically with a Runge–Kutta integration scheme. The multiple shooting method is implemented in the CasADi optimization framework [17]. The interior point method Ipopt [18] is used to solve the optimization problem. The weight was set to $k = 10^{-6}$ to get a nearly time-optimal solution. The time for solving the optimization problem is about 13 s on a standard PC.

5 Experimental results

Experiments are preformed with a Stäubli RX130L robot controlled with a B&R controller system. Detailed hardware description can be found in [8]. The dynamic model of the robot was derived in terms of the base parameters, which were identified with the standard approach using optimized persistent excitation trajectories. A tray is mounted at EE, as shown in Fig. 4, and $N_{Obj} = 2$ cups are placed at the tray. The mass of each cup is $m_{Obj} = 0.12$ kg. The cups have a height of $h = 0.06$ m, and a footprint radius of $r_o = 0.025$ m. For first experiments, the cups are chosen as rigid cylinders to verify the optimization results. The initial and terminal positions of the EE in task space are $\mathbf{r}_{E,0}^T = (-0.11,\ 1.16,\ 0.7)$ m and $\mathbf{r}_{E,e}^T = (-0.11,\ -1.46,\ 0.7)$ m, respectively. In both configurations, the tray is horizontally aligned. The initial and terminal orientation of the tray (i.e. the EE) is described by the vector of Cardan angles $\boldsymbol{\varphi}_{E,0}^T = (0,\ 0,\ 1.56)$ rad and $\boldsymbol{\varphi}_{E,e}^T = (0,\ 0,\ -1.56)$ rad, respectively. The corresponding joint coordinates are determined by solving the inverse kinematics, which yields $\mathbf{q}_0^T = (1.56,\ 0.57,\ -0.20,\ 0,\ -0.36,\ 0)$ rad and $\mathbf{q}_e^T = (-1.56,\ 0.57,\ -0.20,\ 0,\ -0.36,\ 0)$ rad. The positions of the cups relative to the EE-frame are ${}_E\mathbf{r}_{EO1}^T = (0.185,\ 0.075,\ 0.025)$ m, ${}_E\mathbf{r}_{EO2}^T = (0.185,\ -0.075,\ 0.025)$ m, where ${}_E\mathbf{r}_{EOi}$ is the position vector of cup i. Fig. 3 shows the joint trajectory corresponding to the computed time-optimal motion with optimized task duration of $t_e = 1.23$ s. Compared with the time-optimal solution following a prescribed path, which was computed in [8] as $t_e = 1.32$ s, the PtP solution is about 10% faster. The jerks are shown in Fig. 4. The computed feed-forward torque commands and the measured motor torques are shown in Fig. 5, which match well. The importance of a model-based controller is clearly visible, which is also apparent from the small joint tracking error even for this highly dynamic motion. The remaining model uncertainties cause slight deviations at $t = 0.1$ s. This is attributed to elastic effects that are not included in dynamics model. The speed limiting constraints are the friction forces at the cups, as apparent from Fig. 6 (left). The right image in Fig. 6 shows the corresponding normal forces. The limits of the tipping and twisting torques are not active (i.e. they are all negative), see Fig. 7. A video of the experiment can be found at https://youtu.be/C6XpyTvGCAQ

6 Extension to the handling of liquid-filled containers

After successful experimental validation of the proposed method for handling rigid objects placed at the EE, as a further step, the applicability of the obtained trajectory to the handling of liquid-filled containers was tested. To this end, experiments were conducted using (rotationally symmetric conical) plastic coffee cups, which are partially filled with water (Fig. 8). The chosen cup

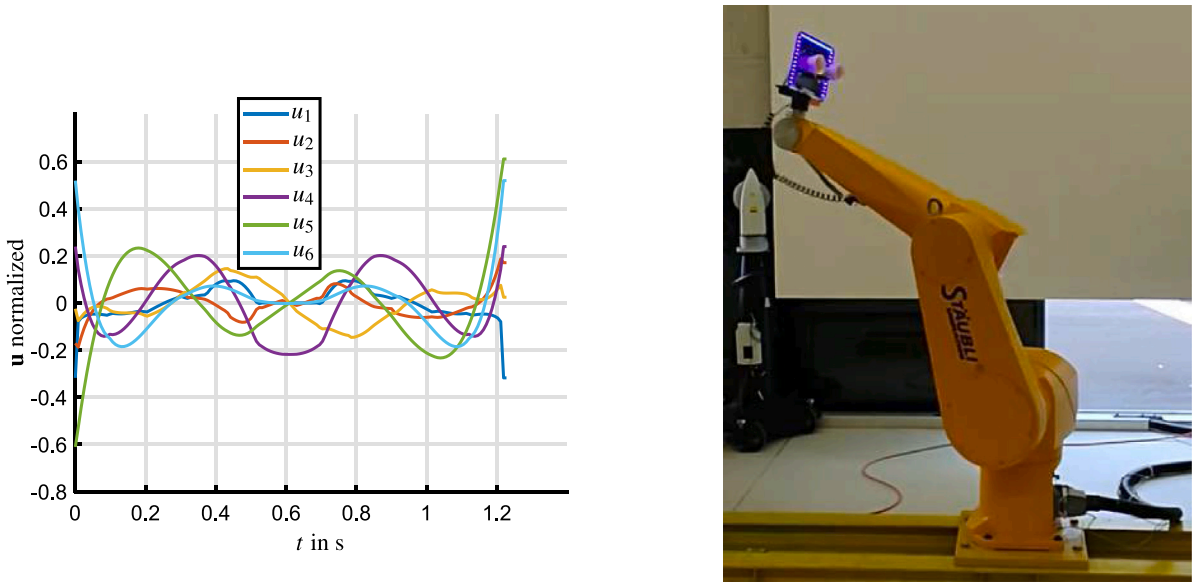

Fig. 4. Jerk $\mathbf{u} = \dddot{\mathbf{q}}$ (left) and a snapshot of an extreme position (right).

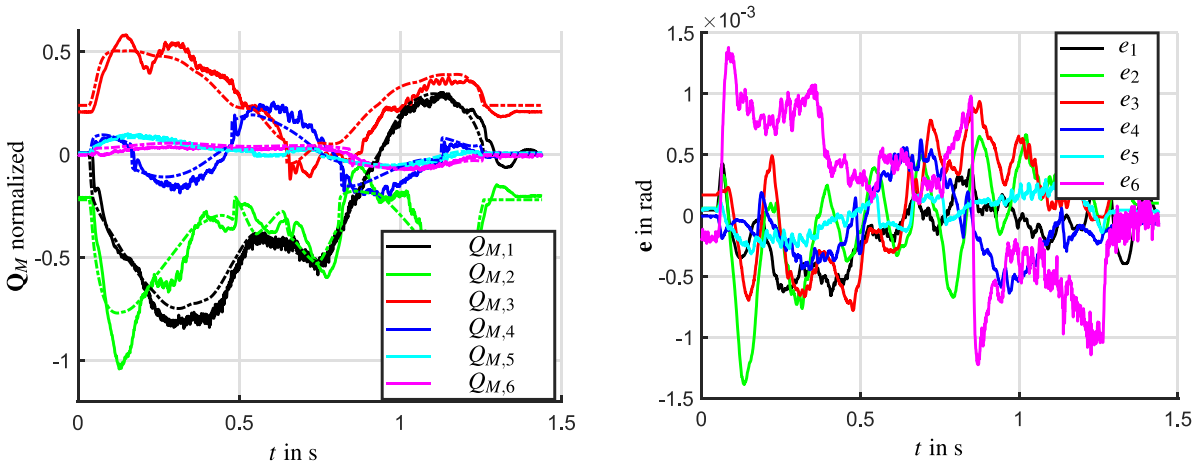

Fig. 5. Measured and computed feed-forward motor torques (left), tracking error (right).

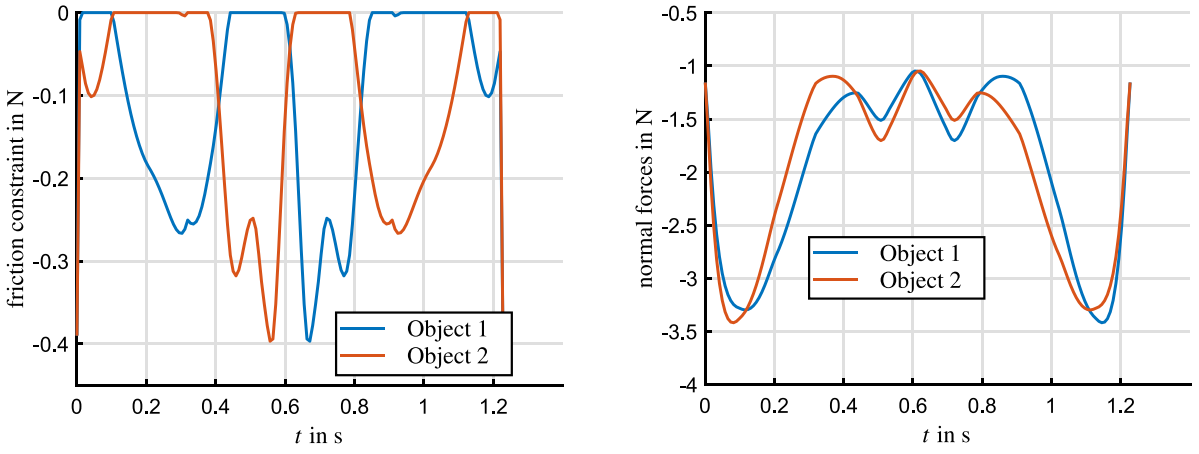

Fig. 6. Friction (left) and normal forces (right).

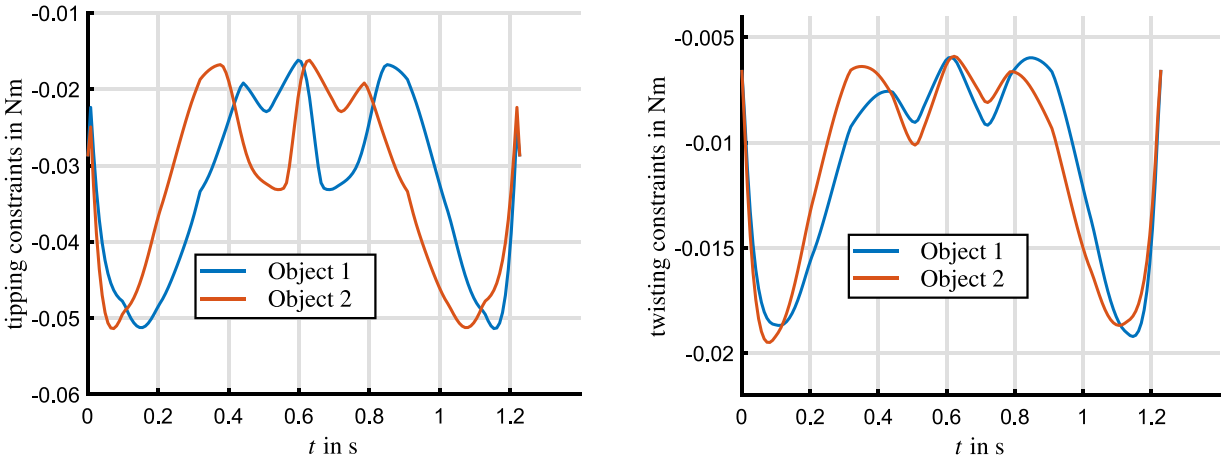

Fig. 7. Tipping (left) and twisting (right) torques.

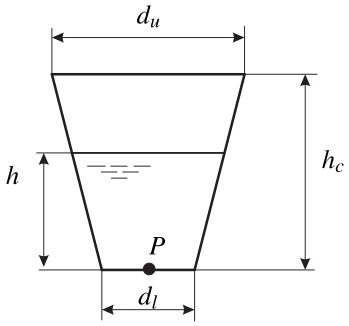

Fig. 8. Geometry of the cup.

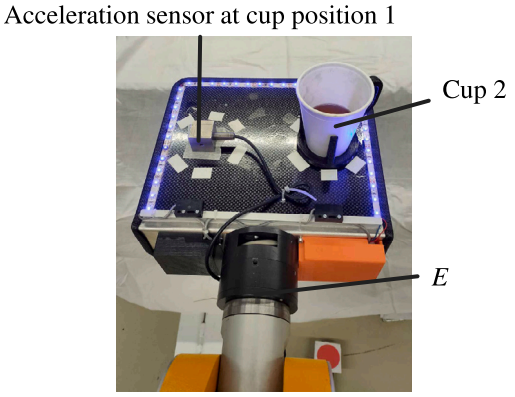

Fig. 9. Tray with acceleration sensor and cup filled with liquid. The cup is stacked to the holder, which is loosely placed at the tray.

has lower and upper diameters of $d_l = 46$ mm, $d_u = 72$ mm and a height of $h_c = 88$ mm. The filling height is indicated with h. Experiments and numerical simulation are carried out to identify the maximal filling height so that no water is spilled out.

The experiments showed that for a filling height above the critical level of $h_{crit} \approx 25$ mm, fluid starts to spill out. The cups remained at their positions, i.e. the constraint as discussed in Section 3 are still met despite the additional dynamic forces due to the sloshing motion of the liquid. Note that this does not hold true for the general case, i.e., for arbitrary container geometries, filling heights, and/or motion trajectories.

To analyze and understand the sloshing behavior in more detail, numerical simulations for the 3D free-surface fluid dynamics were performed using a co-simulation setup between the multibody simulation tool HOTINT [41] and the particle simulation environment LIGGGHTS [42]. The fluid is modeled by means of the meshless particle method SPH [38]. Further details on the

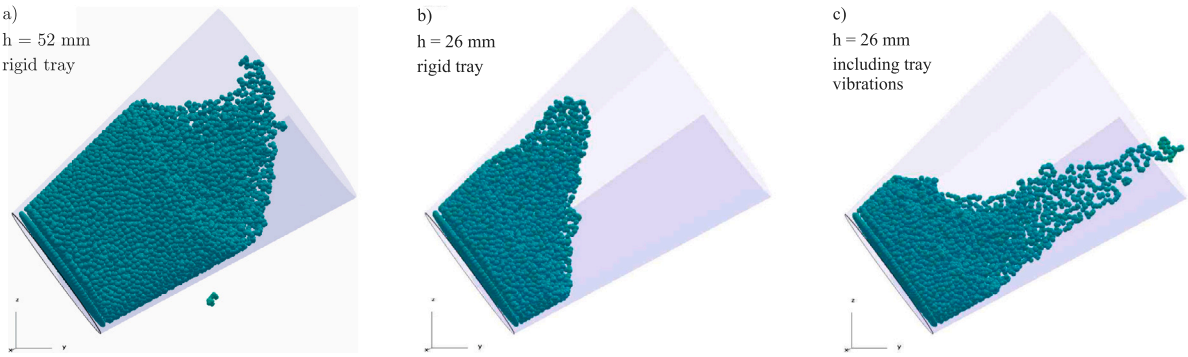

Fig. 10. Snapshot of the SPH simulation at $t = 0.93$ s for cup 2 moving along the computed trajectory. In (a) the initial filling height is $h = 52$ mm, in (b) and (c) it is $h = 26$ mm. Additional harmonic excitation with 5 Hz and 2 m/s^2 was superposed in (c).

numerical formulation and implementation can be found in [24,43,44]. The trajectory computed in Section 5 was imposed as a constrained motion of cup 2 (see Fig. 9). The cup was assumed to be filled with water (density $\rho = 1000$ kg/m^3, kinematic viscosity $\nu = 10^{-6}$ m^2/s) to a defined filling height, and initially oriented upward. Gravity was imposed along the inertial vertical axis.

Simulation were performed with different filling heights. It was found that the liquid started to spill out at $t = 0.93$ s for a filling height of $h = 52$ mm, which is significantly different from the critical height $h_{crit} \approx 25$ mm observed in the experiment. Fig. 10(a) shows a snapshot of the simulation after the liquid separation. The simulation results at the same time instant is shown in Fig. 10(b) for the filling height of $h = 26$ mm, in which case there was no spilling of the liquid.

The discrepancy of measurement and simulation can be attributed to the fact that the used robot is not geometrically calibrated, which can lead to position errors up to 1 cm during motion. However, the dominant cause for the differences is suspected to be the vibrations of the real robot. This is certainly due to the compliance of gears, but it was observed that the tray itself exhibits significant vibrations, which is not accounted for by the model. As a simple means to reflect this effect, a vibratory motion is superimposed to the prescribed tray motion.

To obtain an estimate for the vibratory motion superimposed to the desired trajectory, acceleration measurements were conducted at the EE of the robot. The measurement setup where cup 1 is replaced by an acceleration sensor can be seen in Fig. 9. The measured acceleration and the acceleration according to the desired trajectory (both transformed to the inertial coordinate system (I)) are shown in Fig. 11. The difference of their x-components is shown in Fig. 12, for example, and Fig. 13 shows the frequency spectrum of the acceleration difference. Note that the latter must be interpreted with care, since the frequency resolution and accuracy are low due to the short time span of the dynamic motion. Nevertheless, it becomes clear that the superimposed vibrations have a significant impact on the acceleration profile of the desired trajectory, with acceleration amplitudes somewhere in the range of 1–10 m^2/s.

Parameter studies with harmonic oscillations superimposed to the desired trajectory for different frequencies, amplitudes, and spatial directions were conducted with the 3D CFD simulation, to identify the critical filling height. The highest sensitivity, i.e. the most significant influence of the superimposed vibrations on the critical filling height, was observed for the lowest frequency components in the excitation range. The acceleration magnitude is estimated with 2 m^2/s and the dominant frequency with 5 Hz in all three spatial directions, as deduced from Figs. 11–13. The threshold of the critical filling height, where fluid starts to spill out in the simulation, is approximately 26 mm, which agrees well with the experimentally observed range for h_{crit}. Fig. 10(c) shows the simulation result for filling height $h = 26$ mm when the cup is moving along the time optimal trajectory with the vibration superposed at $t = 0.93$ s.

The time at which the water starts to spill from the cups in the simulation is about $t \approx 0.93$ s, i.e., towards the end of the trajectory, which is also in qualitative agreement with the observations in the experiment. To further validate the simulation, the position where the spilled water is predicted to hit the ground is compared with the position measured in the experiment. Fig. 14 shows the landing position estimated obtained from SPH simulation and the measured position. Also shown is the projection of prescribed trajectory onto the ground with the point indicated where the water separates from the cup. The measured and predicted landing positions are in good agreement, confirming the validity of the SPH model. From these experimental results, it can be concluded that the optimized trajectories satisfying the constraints from Section 3 ensure the safe handling of loosely placed objects, but that additional conditions are necessary in order to avoid sloshing of liquids. Nevertheless, SPH simulation is a powerful method to check sloshing behavior a-posteriori.

7 Conclusion

The waiter motion problem for handling rigid objects was formulated as optimal PtP control problem, and solved with a multiple shooting method. This is a novel approach compared to current the state of research. The formulation accounts for all relevant dynamic phenomena, such as joint friction, limits on the joint rates, accelerations, and jerks, as well as the motor torque. Particularly

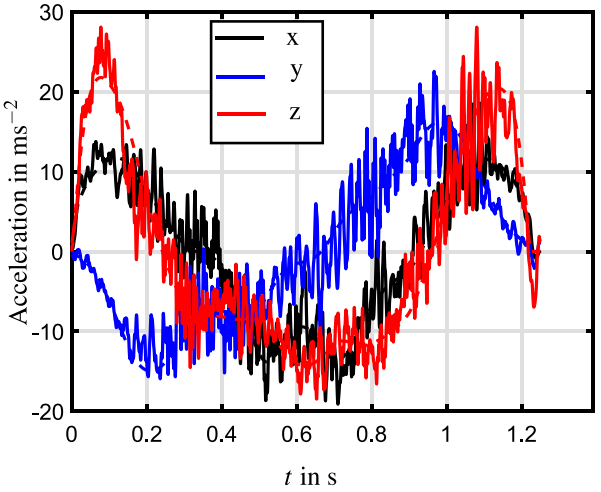

Fig. 11. Measured acceleration of point P of cup 1, and its acceleration according to the desired trajectory (dashed).

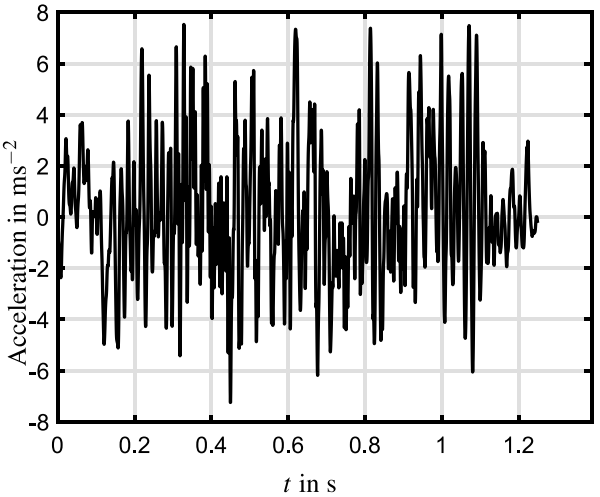

Fig. 12. Difference between measured acceleration and the acceleration of the prescribed trajectories in x-direction.

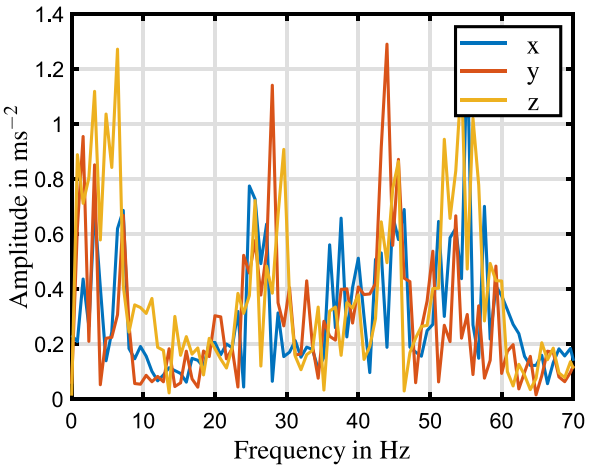

Fig. 13. Fourier transform of the difference between measured and desired acceleration.

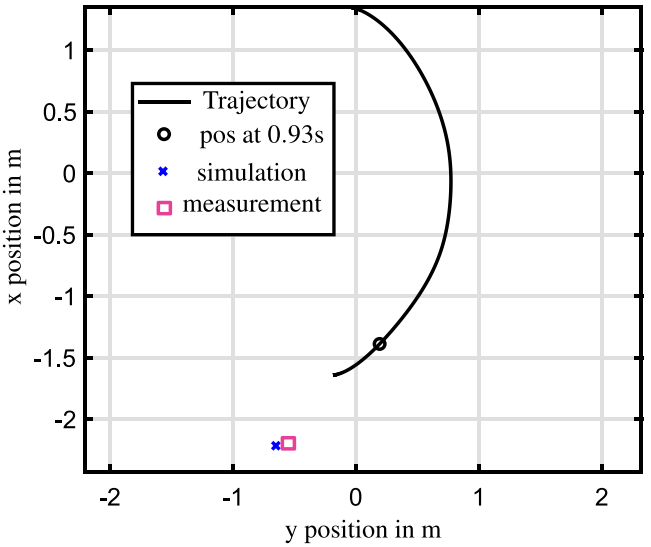

Fig. 14. Trajectory of point P of cup 2. The position where the fluid starts to spill over at $t = 0.93$ s is indicated with ∘. The positions where the fluid hits the ground according to SPH simulation is indicated with ×, and the measured position is indicated with □.

crucial is the modeling of unilateral contact conditions and the corresponding limits. This naturally leads to a non-linear non-convex optimization problem. Experimental results show the feasibility of the computational approach and the practical applicability of the obtained time-optimal trajectories by the example of rigid objects placed at the EE, which can only be ensured by using an identified model. The approach is applicable to general robotic systems including parallel manipulators. Future research will address the improvements of the robot model, in particular so to account for joint/gear compliance. Another extension will be incorporating collision avoidance conditions.

The modular subsystem modeling admits seamless replacement of the EOM of the manipulated objects, and thus to represent the internal dynamics of the objects. This is important in particular when the manipulated objects are liquid-filled containers. Incorporating the fluid dynamics into the optimization problem is subject of future research. In order to investigate the significance of the fluid dynamics, the trajectory obtained for the rigid object was used for handling loosely placed cups filled with water. Results of a physical experiment are compared with results obtained with SPH simulation results. The assumption of a rigid tray was found to be an obvious shortcoming of the robot model. By adding a tray vibration deduced from acceleration measurement, the simulation and measurement data were in good agreement. The results clearly show that superimposing low-frequency vibrations onto the desired trajectory significantly improve the prediction accuracy, despite the many model uncertainties (fluid behavior, container geometry, actual vibration modes, etc.). In order to include the sloshing dynamics in the trajectory optimization, future research will continue to further develop simplified finite-dimensional sloshing models, e.g. [25–27], so account for spatial acceleration and rotation.

Declaration of competing interest

The authors declare that they have no known competing financial interests or personal relationships that could have appeared to influence the work reported in this paper.

Data availability

No data was used for the research described in the article.

Acknowledgments

This work has been supported by the “LCM-K2 Center for Symbiotic Mechatronics” within the Austrian COMET-K2 program.

References

[1] F. Geu Flores, A. Kecskeméthy, Time-optimal path planning for the general waiter motion problem, in: Advances in Mechanisms, Robotics and Design Education and Research, Springer Verlag, 2013, pp. 189–203.
[2] F. Geu Flores, A. Kecskeméthy, A. Pöttker, Time-optimal motion planning along specified paths for multibody systems including dry friction and power constraints, in: 13th World Congress in Mech. Mach. Science, 2011.

[3] M. Oberherber, H. Gattringer, K. Springer, A time optimal solution for the waiter motion problem with an industrial robot, in: Proceedings of the Austrian Robotics Workshop (ARW) 2013, 2013, pp. 55–60.
[4] F. Debrouwere, W. Loock, G. Pipeleers, M. Diehl, J. Swevers, J. Schutter, Convex time-optimal robot path following with Cartesian acceleration and inertial force and torque constraints, J. Syst. Control Eng. 227 (2013) 724–732.
[5] G. Csorvási, A. Nagy, I. Vajk, Near time-optimal path tracking method for waiter motion problem, IFAC-PapersOnLine 50 (1) (2017) 4929–4934.
[6] Á. Nagy, G. Csorvási, I. Vajk, Path tracking algorithms for non-convex waiter motion problem, Period. Polytech. Electr. Eng. Comput. Sci. 62 (1) (2018) 16–23.
[7] H. Gattringer, A. Müller, M. Oberherber, D. Kaserer, Time-optimal path following for robotic manipulation of loosely placed objects: Modeling and experiment, in: 21th IFAC World Congress, Vol. 53, 2020, pp. 8450–8455, (2).
[8] H. Gattringer, A. Müller, M. Oberherber, D. Kaserer, Time-optimal robotic manipulation on a predefined path of loosely placed objects: Modeling and experiment, Mechatronics 84 (2022) 102753.
[9] N. Van Duijkeren, F. Debrouwere, G. Pipeleers, J. Swevers, Cartesian constrained time-optimal point-to-point motion planning for robots: The waiter problem, in: Benelux Meeting on Systems and Control. Belgium, 2015.
[10] H. Pham, Q.-C. Pham, Critically fast pick-and-place with suction cups, in: 2019 Int. Conf. Rob. Automat. (ICRA), IEEE, 2019, pp. 3045–3051.
[11] Q.-C. Pham, S. Caron, Y. Nakamura, Kinodynamic planning in the configuration space via admissible velocity propagation, in: Proceedings of Robotics: Science and Systems, 2013.
[12] J. Luo, K. Hauser, Robust trajectory optimization under frictional contact with iterative learning, in: Robotics, Science and Systems (RSS), 2015.
[13] G. Csorvási, I. Vajk, Sequential time-optimal algorithm for extended path tracking problem, J. Dyn. Syst. Meas. Control 142 (2020) 081005.
[14] C. Troll, S. Tietze, J.-P. Majschak, Controlling liquid slosh by applying optimal operating-speed-dependent motion profiles, Robotics 9 (1) (2020) 18.
[15] L. Moriello, L. Biagiotti, C. Melchiorri, A. Paoli, Manipulating liquids with robots: A sloshing-free solution, Control Eng. Pract. 78 (2018) 129–141.
[16] R.C. Muchacho, R. Laha, L. Figueredo, S. Haddadin, A solution to slosh-free robot trajectory optimization, in: 2022 IEEE/RSJ International Conference on Intelligent Robots and Systems (IROS), IEEE, 2022, pp. 223–230.
[17] J.A.E. Andersson, J. Gillis, G. Horn, J.B. Rawlings, M. Diehl, CasADi – A software framework for nonlinear optimization and optimal control, Math. Program. Comput. 11 (1) (2019) 1–36.
[18] A. Wächter, L. Biegler, On the implementation of a primal-dual interior point filter line search algorithm for large-scale nonlinear programming, Math. Program. 106 (2006) 25–57.
[19] R.A. Ibrahim, V.N. Pilipchuk, T. Ikeda, Recent Advances in Liquid Sloshing Dynamics, Appl. Mech. Rev. 54 (2) (2001) 133–199.
[20] H. Gao, K. Kwok, B. Samali, Optimization of tuned liquid column dampers, Eng. Struct. 19 (6) (1997) 476–486.
[21] M. Toumi, M. Bouazara, M. Richard, Impact of liquid sloshing on the behaviour of vehicles carrying liquid cargo, Eur. J. Mech. A Solids 28 (2009) 1026–1034.
[22] K. Yano, K. Terashima, Robust liquid container transfer control for complete sloshing suppression, IEEE Trans. Control. Syst. Technol. 9 (2001) 483–493.
[23] L. Moriello, L. Biagiotti, C. Melchiorri, A. Paoli, Manipulating liquids with robots: a sloshing-free solution, Control Eng. Pract. 78 (2018) http://dx.doi.org/10.1016/j.conengprac.2018.06.018.
[24] M. Schörgenhumer, A. Eitzlmayr, Modeling of liquid sloshing with application in robotics and automation, IFAC-PapersOnLine 52 (15) (2019) 253–258.
[25] J. Schröck, J. Wenninger, E. Karer, A. Eitzlmayr, Modeling, simulation, and experimental analysis of liquid sloshing dynamics, in: Dynamics and Control of Advanced Structures and Machines, Springer, 2022, pp. 219–231.
[26] R. Di Leva, M. Carricato, H. Gattringer, A. Müller, Sloshing dynamics estimation for liquid-filled containers under 2-dimensional excitation, in: ECCOMAS Thematic Conference on Multibody Dynamics, 2021, pp. 80–89.
[27] R. Di Leva, M. Carricato, H. Gattringer, A. Müller, Time-optimal trajectory planning for anti-sloshing 2-dimensional motions of an industrial robot, in: 2021 20th International Conference on Advanced Robotics (ICAR), IEEE, 2021, pp. 32–37.
[28] I.A. Raouf, Liquid Sloshing Dynamics: Theory and Applications, Cambridge University Press, 2005.
[29] L. Battaglia, M. Cruchaga, M. Storti, J. D'Elía, J. Núñez Aedo, R. Reinoso, Numerical modelling of 3D sloshing experiments in rectangular tanks, Appl. Math. Model. 59 (2018) 357–378.
[30] M. Konopka, F. De Rose, H. Strauch, C. Jetzschmann, N. Darkow, J. Gerstmann, Active slosh control and damping - Simulation and experiment, Acta Astronaut. (2019).
[31] N. Chentanez, M. Müller, Real-time Eulerian water simulation using a restricted tall cell grid, ACM Trans. Graph. 30 (2011) 82, http://dx.doi.org/10.1145/2010324.1964977.
[32] J.R. Shao, H.Q. Li, G.R. Liu, M.B. Liu, An improved SPH method for modeling liquid sloshing dynamics, Comput. Struct. 100–101 (2012) 18–26.
[33] M.D. Green, J. Peiró, Long duration SPH simulations of sloshing in tanks with a low fill ratio and high stretching, Comput. & Fluids 174 (2018) 179–199.
[34] J. Fonfach, T. Manderbacka, M. Neves, Numerical sloshing simulations: Comparison between lagrangian and lumped mass models applied to two compartments with mass transfer, Ocean Eng. 114 (2016) 168–184.
[35] S. Rebouillat, D. Liksonov, Fluid–structure interaction in partially filled liquid containers: A comparative review of numerical approaches, Comput. & Fluids 39 (2010) 739–746, http://dx.doi.org/10.1016/j.compfluid.2009.12.010.
[36] R. Di Leva, M. Carricato, H. Gattringer, A. Müller, Sloshing dynamics estimation for liquid-filled containers performing 3-dimensional motions: modeling and experimental validation, Multibody Syst. Dyn. 56 (2) (2022) 153–171.
[37] L.B. Lucy, A numerical approach to the testing of the fission hypothesis, Astron. J. 82 (1977) 1013–1024.
[38] J. Monaghan, Simulating free surface flows with SPH, J. Comput. Phys. 110 (2) (1994) 399–406.
[39] J.J. Monaghan, Smoothed Particle Hydrodynamics, Rep. Progr. Phys. 68 (2005) 1703, http://dx.doi.org/10.1088/0034-4885/68/8/R01.
[40] M. Liu, G. Liu, Smoothed particle hydrodynamics (SPH): an overview and recent developments, Arch. Comput. Methods Eng. 17 (2010) 25–76, http://dx.doi.org/10.1007/s11831-010-9040-7.
[41] J. Gerstmayr, A. Dorninger, R. Eder, P. Gruber, D. Reischl, M. Saxinger, M. Schörgenhumer, A. Humer, K. Nachbagauer, A. Pechstein, Y. Vetyukov, HOTINT: A Script Language Based Framework for the Simulation of Multibody Dynamics Systems, in: International Design Engineering Technical Conferences and Computers and Information in Engineering Conference, Volume 7B: 9th International Conference on Multibody Systems, Nonlinear Dynamics, and Control, 2013, V07BT10A047.
[42] C. Kloss, C. Goniva, A. Hager, S. Amberger, S. Pirker, Models, algorithms and validation for opensource DEM and CFD–DEM, Prog. Comput. Fluid Dyn. Int. J. 12 (2–3) (2012) 140–152.
[43] M. Schörgenhumer, P. Gruber, J. Gerstmayr, Interaction of flexible multibody systems with fluids analyzed by means of smoothed particle hydrodynamics, Multibody Syst. Dyn. 30 (2013) http://dx.doi.org/10.1007/s11044-013-9359-6.
[44] M. Schörgenhumer, A. Humer, Smoothed particle hydrodynamics and modal reduction for efficient fluid–structure interaction, Math. Comput. Model. Dyn. Syst. 24 (2018) 387–408, http://dx.doi.org/10.1080/13873954.2018.1488739.
[45] W. Khalil, E. Dombre, Modeling, Identification and Control of Robots, Hermes Penton, London, 2002.
[46] M. Neubauer, H. Gattringer, H. Bremer, A persistent method for parameter identification of a seven-axes manipulator, Robotica 33 (2014) 1099–1112.